

# ANALYSIS OF AIRBORNE HYPERSPECTRAL IMAGE USING VEGETATION INDICES, RED EDGE POSITION AND CONTINUUM REMOVAL FOR DETECTION OF *Ganoderma* DISEASE IN OIL PALM

IZZUDDIN, M A\*; NISFARIZA, M N\*\*; EZZATI, B\*\*; IDRIS, A S\*; STEVEN, M D<sup>†</sup> and BOYD, D<sup>‡</sup>

## ABSTRACT

The basal stem rot (BSR) of oil palm caused by *Ganoderma* has brought huge losses to the oil palm industry in Malaysia. Airborne hyperspectral remote sensing technology may provide assistance to detect and classify different categories of *Ganoderma* disease severity index (DSI) in oil palm. In this study, five common vegetation indices (VI), four red edge position (REP) and four continuum removal (CR) were applied to categorise oil palm into T1 (healthy), T2 (mild) and T3 (severe) infection of *Ganoderma* disease in oil palm. The accuracy of the VI, REP and CR were assessed using confusion matrix and t-test. The results revealed that two VI, i.e. Simple Ratio Index (SRI) and Enhanced Vegetation Index (EVI) have moderate capability for the detection of *Ganoderma* disease in oil palm. SRI showed moderate classification accuracy (44.4%) compared to EVI with 40.7% accuracy; while the other three VI had poor accuracy (<40%). The analysis of REP using t-test showed that none of the REP could differentiate between T1 vs. T2 significantly, but differences between T1 vs. T3 and T2 vs. T3 are statistically obvious. Meanwhile analysis using CR gave promising results when there are statistical significant differences between T1 vs. T2 in the 500 nanometer (nm) absorption region of Band Depth Normalised to Area (BDNA). In conclusion, the common VI and REP generated from airborne hyperspectral image had low to moderate accuracy for detection of *Ganoderma* disease. Meanwhile, CR gave promising results for early detection of the disease. Further analysis must be conducted to validate and ensure the robustness of the results and also should look towards generating specific spectral indices and bi-directional reflectance (BRDF) model for detection of *Ganoderma* disease in oil palm.

**Keywords:** hyperspectral, *Ganoderma*, vegetation indices, red edge position, continuum removal.

**Date received:** 20 April 2017; **Sent for revision:** 21 April 2017; **Received in final form:** 26 March 2018; **Accepted:** 5 July 2018.

\* Malaysian Palm Oil Board, 6 Persiaran Institusi,  
Bandar Baru Bangi, 43000 Kajang,  
Selangor, Malaysia.  
E-mail: idris@mpob.gov.my

\*\* Department of Geography, Faculty of Arts and Social Sciences,  
Universiti Malaya, Jalan Universiti,  
50603 Kuala Lumpur, Malaysia.

† School of Geography, Faculty of Social Sciences,  
Sir Clive Granger Building,  
University of Nottingham, University Park, Nottingham NG72RD,  
United Kingdom.

## INTRODUCTION

*Ganoderma* disease infections have caused serious decrease of oil palm yield in Malaysia. It rapidly results in high yield losses and oil quality reductions (Roslan and Idris, 2012) because the infected oil palms were damaged and unable to transfer water and nutrients from the roots to the stem, fronds, leaves and fruits (Nuranis *et al.*, 2016). Moreover, the

*Ganoderma* fungus can infect other oil palm by root to root contact (Idris *et al.*, 2016). Hence, there is an urgent need to identify infected oil palm and apply control measures to kill the fungus before infecting other oil palms. If the symptoms of the *Ganoderma* disease could be detected early, at least prior to emergence of foliar symptoms, the planters would indeed be able to treat the infected oil palm early and prolonging the economic life of the oil palm.

Currently, ground assessment of the *Ganoderma* disease is made using visual inspection based on the appearance of *Ganoderma* mycelium, small white button, fruiting bodies on stem and bole rotting at the palm base and also the foliar symptoms such as yellowing and drying of leaves and skirting of lower fronds of the oil palm canopy (Idris *et al.*, 2016). Hence, these oil palm physiological changes may lead to pronounced variations in spectral properties of infected oil palm. Ground assessment of *Ganoderma* disease makes it difficult to accurately estimate the regional distribution and severity of the disease in large areas within a short time. This method is labour-intensive and time-consuming. There is a need to develop an aerial detection technology to detect *Ganoderma* disease in large area of oil palm plantation.

The utilisation of spectral analysis for detection of fungal and bacterial diseases is currently under extensive investigation (Mahlein *et al.*, 2010; Lelong *et al.*, 2010; Shafri *et al.*, 2009). Both fungi and bacteria usually cause damages at molecular, tissue and cellular stages leading to changes in the spectral signatures (Gupta, 2010). These changes of spectral signatures become key indicator to differentiate between healthy and disease oil palm. On the other hand, Franke *et al.* (2005) stressed that hyperspectral imaging provided considerable advantages over multispectral approaches for the detection of wheat leaf rust. The combination of spectral and spatial information provided by image analysis facilitates detection of plant diseases and infection-related damages in crops (Rogge *et al.*, 2007). Furthermore, Xing *et al.* (2005) indicated that a utilisation of hyperspectral wavebands could detect bruises in 'Golden Delicious' apple with high accuracy. These studies show opportunity for utilisation of hyperspectral remote sensing for detection of *Ganoderma* disease in oil palm.

Regarding *Ganoderma* disease infections in oil palm, Izzuddin (2010) had developed several new spectral indices for *Ganoderma* disease detection in oil palm seedlings, yet no extensive study had been made to test the spectral indices on airborne hyperspectral image. In other approaches, Nisfariza (2012) had studied the capability of airborne hyperspectral and field spectroscopy for detection of *Ganoderma* disease in oil palm. The findings of their studies also have been documented in Shafri and Hamdan (2009) and Shafri *et al.* (2011a, b).

Currently, researches on detection of *Ganoderma* disease in oil palm mainly focus on laboratory-based approaches (Madihah *et al.*, 2014). However, for practical applications, it is essential to identify *Ganoderma* disease at a very early stage or mild infection in the field. Only this will give a realistic chance to successfully solve this important economic and food source problems. Early detection of the disease via aerial view can strongly assist the reduction of losses. Although, *Ganoderma* disease only infect the root and base of the oil palm stem, but a study by Haniff *et al.* (2005) has motivated the use of aerial detection of *Ganoderma* disease in oil palm. Haniff *et al.* (2005) studied the gas exchange response of oil palm to *Ganoderma* disease and suggested that early infection of *Ganoderma* at the oil palm root triggered the root chemical signaling such as abscisic acid (ABA) produced by dehydrating roots even when the water status in the field is kept constant. The chemical signal caused stomata closure as a direct response. The stomata closure resulted in reduction of stomatal conductance which was highly correlated to photosynthesis ( $R^2 = 0.896$ ). These physiological changes in oil palm foliar should cause spectral changes over time.

However, appropriate operating procedures in using airborne hyperspectral remote sensing for detection of the infected oil palm in the field are still not extensively studied and validated. Hence, the objective of the study was to analyse and assess the airborne hyperspectral image using vegetation indices (VI), red edge position (REP) and continuum-removal (CR) for detection of *Ganoderma* disease in oil palm.

## MATERIALS AND METHODS

### Study Area

The study plot was located in an oil palm plantation in Seberang Perak, Perak, Malaysia ( $4^\circ 6' 42''$  N and  $100^\circ 53' 12''$  E) in Figure 1 with annual precipitation of 2256 mm per year and temperature between  $24^\circ\text{C}$  -  $34^\circ\text{C}$ . The size of the area is estimated to be around 25 ha and planted with *Dura x Pisifera* (DxP) oil palm planting materials.

The planting density of the plot is 160 oil palms per hectare and age of the oil palms was 17 years old. The area was selected due to the good management practice, relatively flat terrain with no other diseases, pest infestation and nutrient deficiencies.

### Ground Data Collection

The ground data collection involved fieldworks to record *Ganoderma* disease census and collection of geographic coordinates using global positioning system (GPS) on several landmarks in the study

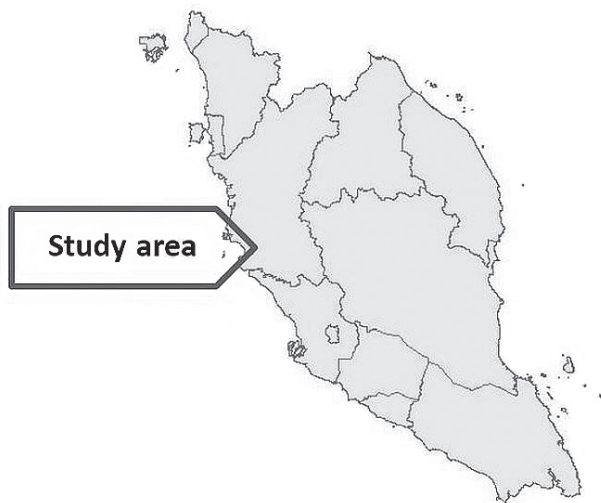


Figure 1. Location of study area.

plot for image geometric correction input. The *Ganoderma* disease census in the plot was conducted for a duration of five days in October 2008 during the airborne data acquisition campaign. The oil palms, categorised into three *Ganoderma* disease severity index (DSI), were labelled as T1 (healthy), T2 (mild) and T3 (severe) (Table 1). The oil palms were categorised into DSI based on visual symptoms of the disease that appear on the oil palm (Table 1). About 27 oil palms were selected for sampling of spectral signatures for each category of the *Ganoderma* disease. Nine oil palms per category were selected for the image processing. The spectral signatures were extracted and stored in Environment for Visualising Images (ENVI) (version 4.8, ITT VSI, White Plains, NY, USA) software for processing and analysis.

### Airborne Hyperspectral

The airborne hyperspectral images were acquired in October 2008 over the study area by using Airborne Imaging Spectrometer for Applications (AISA) Dual hyperspectral imaging system that was mounted on aircraft type Short SC-7 Skyvan, a twin-engine turboprop cargo aircraft. The sensor was developed and manufactured by SPECIM (Spectral Imaging Limited), Finland. The system provides

hyperspectral image within wavelength range of 401 nm – 997 nm, with 128 bands and 0.68 m ground spatial resolution at 1000 m of flight altitude. The image was acquired between 2.00 pm – 4.00 pm local time with cloudy skies and fluctuations in illumination but with high visibility (40 km) measured by the aircraft personnel. The airborne data acquisition had to be conducted during cloudy skies due the starting of east-coast monsoon season in the month of October that bring high amount of clouds and the limited time of chartered aircraft availability. Any delay of chartering the aircraft shall increase the cost for data acquisition. The dynamics of reflectance the image that caused by different sunlight intensity during the cloudy skies can be corrected using the QUAC module in ENVI 4.8 software.

### Pre-processing

The raw hyperspectral images were radiometrically calibrated to radiance and then atmospherically corrected to reflectance by Quick Atmospheric Correction Code (QUAC) module in ENVI 4.8 software. The QUAC module was applied on each individual raw image before mosaicking and orthophoto processes were conducted. The final reflectance values were measured in percentage unit (0%-100%). The calibrated data were then georeferenced using ground coordinate obtained from GPS and inertial measurement unit (IMU) information. The final mosaic image which was georeferenced in Rectified Skewed Orthomorphic (RSO) projection of West Malaysia with Kertau 48 as datum (Figure 2).

### Processing

The hyperspectral image was applied with five vegetation indices (VI). The VI is a combination of surface reflectance at two or more wavelengths designed to highlight a particular property of vegetation and to describe plant foliage. In this study, the hyperspectral image was transformed into VI using the Vegetation Analysis Tool provided in ENVI version 4.8 software. Based on the literature reviews, several VI were selected for evaluation with the hyperspectral image (Table 2).

TABLE 1. *Ganoderma* DISEASE SEVERITY INDEX (DSI) CATEGORY

Label	Category	Visual symptoms
T1	Healthy	Oil palm looks healthy, no foliar symptom, absence of <i>Ganoderma</i> white mycelium and fruiting bodies at the palm base.
T2	Mild	Oil palm looks healthy, but presence of <i>Ganoderma</i> white mycelium, small white button or fruiting bodies at the palm base. No stem and bole rotting at the palm base.
T3	Severe	Two or more unopened spear leaves, old fronds snapping at the petiole and drooping, yellowing of leaves, existence of <i>Ganoderma</i> fruiting bodies, stem and bole rotting at the palm base.

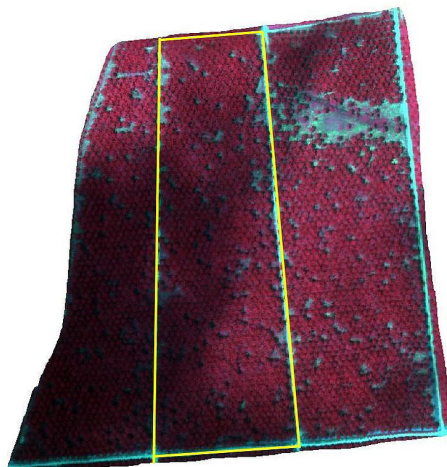


Figure 2. Pre-process airborne hyperspectral image.

The Normalised Difference Vegetation Index (NDVI) algorithm normalises the differences between reflectance from Red (R) and near infrared (NIR) band that may come from different illumination fluctuations caused by environment such as cloud shades and bright areas. NDVI is also used for leaf area index (LAI), biomass, percentage vegetation cover and absorbed photosynthetically active radiation (PAR) and wheat leaf rust (*Puccinia triticina*) disease detection in wheat (*Triticum dicoccum*) (Ashourloo *et al.*, 2014). The NDVI values ranges from -1.0 to 1.0 where -1.0 represents very low level of vegetation greenness and 1.0 represents very high level of vegetation greenness.

Simple Ratio Index (SRI) range of values is from 0.0 to more than 30, where healthy vegetation

TABLE 2. LIST OF VEGETATION INDICES

No .	Vegetation indices	Algorithm	Reference	Primary application
1.	Normalised Difference Vegetation Index (NDVI)	$NDVI = \frac{NIR - Red}{NIR + Red}$	Rouse <i>et al.</i> (1974); Daughtry <i>et al.</i> (2000)	Assessment of green biomass.
2.	Simple Ratio Index (SRI)	$SRI = \frac{NIR}{Red}$	Jordan (1969)	Estimation of chlorophyll content and green biomass.
		where: NIR = reflectance ranges from 750 nm – 900 nm Red = reflectance ranges from 660 nm – 720 nm The inverse of the relationship is also possible.		
3.	Enhanced Vegetation Index (EVI)	$EVI = G \times \frac{\rho_{nir} - \rho_{red}}{\rho_{nir} + (C_1 \times \rho_{red} - C_2 \times \rho_{blue})} + L$	Liu and Huete (1995)	Enhanced estimate chlorophyll content.
		where: $L$ = soil adjustment factor. $C_1$ and $C_2$ = coefficients used to correct aerosol scattering in the Red band using Blue band. $\rho_{blue}$ = reflectance at Blue band (450 nm – 0.52 nm). $\rho_{red}$ = reflectance at Red band (600 nm – 700 nm). $\rho_{nir}$ = reflectance at near infrared band (700 – 1100 nm).		
4.	Vogelmann Red Edge Index (VOG1)	$VOG1 = \frac{\rho_{740}}{\rho_{720}}$	Vogelmann <i>et al.</i> (1993)	Narrowband reflectance measurement that is sensitive to the combined effects of foliage chlorophyll concentration, canopy leaf area and water content.
		where: $\rho_{740}$ = reflectance at wavelength 740 nm. $\rho_{720}$ = reflectance at wavelength 720 nm.		
5.	Carotenoid Reflectance Index 2 (CRI2)	$CRI2 = \frac{1}{\rho_{510}} - \frac{1}{\rho_{700}}$	Gitelson <i>et al.</i> (2005)	Enhanced estimation of concentration of carotenoids relative to chlorophyll.
		where: $\rho_{510}$ = reflectance at wavelength 510 nm. $\rho_{700}$ = reflectance at wavelength 700 nm.		

usually has values of 2 to 8. SRI has also been used for disease detection (Vogelmann *et al.*, 1993; Calderon *et al.*, 2013). Vogelmann *et al.* (1993) tested the SRI in hyperspectral data from sugar maple leaves that suffered from extensive insect damage. They concluded that SRI is varied among populations of sugar maples and over the growing season, but did not correlate well with total chlorophyll content. Calderon *et al.* (2013) tested SRI and obtained significant difference between healthy and *Verticillium wilt* infected olive with *p*-value of 0.001 and F-statistics of 14.35 when tested using analysis of variance (ANOVA).

The Enhanced Vegetation Index (EVI) decouples the canopy background signal and measures reduction in atmosphere influences. This index is more responsive to canopy structural variations. The range of values for the EVI is -1 to 1, where healthy vegetation generally falls between values of 0.20 to 0.80. EVI enhances the vegetation spectral features in high biomass regions. Phadikar and Goswami (2016) used EVI for automatic classification of brown spot and blast disease in rice. Their results suggest good overall accuracy of detection of the disease with 80%–86% accuracy using 14 different types of image classifiers. In another study, Sankaran and Ehsani (2011) used EVI to detect citrus greening. The results showed that EVI provided  $83 \pm 5\%$  overall accuracy for disease detection.

Another VI is Vogelmann Red Edge Index 1 (VOG1) with the range of VOG1 values from 0-20 and the common range of vegetation area is 4 to 8 (Vogelmann *et al.*, 1993). The red edge is primarily used to assess the chlorophyll content of vegetation. But there are studies that used REP for crop disease detection (Clevers and Gitelson, 2013; Krezhova *et al.*, 2014).

The Carotenoid Reflectance Index 2 (CRI2) is sensitive to carotenoid pigments in plant foliage (Gitelson *et al.*, 2002). The carotenoids help plants absorb light energy for use in photosynthesis and diseased vegetation usually contains lower carotenoid concentrations (Filimon *et al.*, 2016). Zhao *et al.* (2016) studied the content of carotenoid and chlorophyll in cucumber leaves infected by angular leaf spot disease. Their study suggested that there is significant decrease in carotenoid and chlorophyll contents in cucumber leaves after infection.

The VI outputs in form of one-band image were then classified into T1, T2 and T3 using manual density slicing technique specifically within designated threshold of values of each index for each disease category. Density slicing is a simple classification technique for single band image where a range of input pixel from VI values is mapped to a single pixel value that correspond to T1, T2 and T3 category. These classifications resulted in pseudocolour image output where each disease

category was assigned to different colour scheme. Density slicing commonly used where the pixel values have direct relationship to physical variable (Rees, 2013).

Other than the VI, four types of Red Edge Position (REP) were also used in this study. The REP is located between 680 nm and 750 nm and is defined as the wavelength of the inflection point of the reflectance at the red edge slope. Previous studies indicate that the REP is related to foliar chlorophyll contents and provides a very sensitive indicator of vegetation stress. Haniff *et al.* (2005) mentioned that *Ganoderma* infected oil palm relative chlorophyll content is lower than healthy oil palm with 10.3% reduction. Thus, justify the potential of REP for detection of *Ganoderma* disease in oil palm. The REP is determined by the combined effects of chlorophyll absorption and leaf internal scattering (Cho and Skidmore, 2006).

The REP is a unique feature of green vegetation because it results from two special optical properties of plant tissue, high internal leaf scattering causing large NIR reflectance and chlorophyll absorption giving low R reflectance (Cho and Skidmore, 2006). The REP is almost certainly one of the best known and most widely used parameters in relating chlorophyll content to vegetation spectral reflectance (Wu *et al.*, 2009).

This red edge feature is the transition zone on the steep change in reflectance between the strong chlorophyll absorption near 680 nm and the strong scattering by leaf cell structure from 750 nm, which has been measured on leaves of various species by first derivative reflectance spectrometry (Haboudane *et al.*, 2002). It is easily noticed as a large peak in the first derivative of a narrowband reflectance spectral curve, representing the point of maximum slope. REP also can provide status on chlorophyll content, biomass and hydric status of plants (Filella and Penuelas, 1994).

Several studies have discussed the methodology in obtaining the REP in vegetation (Carter and Knapp, 2001; Cho and Skidmore, 2006; Vincini and Frazzi, 2011). Generally, four methods of identifying REP have been used by researchers to identify the red edge in the remote sensing literature. *Table 3* shows the REP used in this study.

Continuum Removal (CR) was also applied in the image analysis. CR analysis was first used in the study of mineral composition and discrimination (Clark and Roush 1984; Kokaly and Clark, 1999) whereby the use of continuum-removed spectra was embedded in the Spectral Feature Fitting (SFF) algorithm. The CR techniques for vegetation were first introduced by Kokaly and Clark (1999). The essence of feature selection lies in the isolation of the absorption features from the rest of the spectrum using a continuum line. There are four CR used in this study as in *Table 4*.

**TABLE 3. LIST OF RED EDGE POSITION**

Red Edge Position (REP)	Algorithm	References
Linear Interpolation (LI)	$LI = 700 + 40 \left( \frac{R_{edge} - R_{700}}{R_{740} - R_{700}} \right)$ where: $R_{edge} = \frac{(R_{670} + R_{780})}{2}$	Guyot <i>et al.</i> (1992); Clevers (1994)
Inverted Gaussian [R( $\lambda$ )]	$R(\lambda) = R_s - (R_s - R_o) e^{\frac{(\lambda - \lambda_o)^2}{2\sigma^2}}$	Bonham-Carter (1988); Miller <i>et al.</i> (1990)
Three Point Langrangian ( $D_\lambda$ )	$D_\lambda = \frac{(\lambda - \lambda_i)(\lambda - \lambda_{i+1})}{(\lambda_{i-1} - \lambda_i)(\lambda_{i-1} - \lambda_{i+1})} D_{\lambda(i-1)} + \frac{(\lambda - \lambda_{i-1})(\lambda - \lambda_{i+1})}{(\lambda_i - \lambda_{i-1})(\lambda_i - \lambda_{i+1})} D_{\lambda(i)} + \frac{(\lambda - \lambda_{i-1})(\lambda - \lambda_i)}{(\lambda_{i+1} - \lambda_{i-1})(\lambda_{i+1} - \lambda_i)} D_{\lambda(i+1)}$	Dawson and Curran (1998)
Maximum First Derivative ( $FDR_{\lambda_i}$ )	$FDR_{\lambda_i} = \frac{(R_{\lambda(i+1)} - R_{\lambda(i)})}{\Delta\lambda}$	Dawson and Curran (1998)

**TABLE 4. LIST OF CONTINUUM REMOVAL**

Continuum removal (CR)	Algorithm
Continuum Removed Reflectance (CRR)	$CRR = \frac{R}{CR}$
Band Depth (BD)	$BD = 1 - CRR$
Normalised Band Depth (NBD)	$NBD = \frac{BD}{BD_c}$
Band Depth Normalised to Area (BDNA)	$BDNA = \frac{BD}{\sum BD}$

The CR is used to normalise reflectance spectra to compare individual absorption features from a common baseline. The continuum is a convex hull fit over the top of a spectrum using straight-line segments that connect local spectra maxima. The first and last spectral data values are on the hull; therefore, the first and last bands in the output continuum-removed data file are equal to 1.0 (Clark, 2003).

Mutanga and Skidmore (2003) found that the application of CR to vegetation spectra data improves the statistical difference between vegetation types in the visible spectrum, but weakens the statistical difference of the spectra in NIR and shortwave infrared part of the spectrum. The CR indices are less sensitive to underlying soil surface and fractional canopy coverage (Kokaly and Clark, 1999). The CR analysis on the hyperspectral image was conducted using ENVI 4.8 software.

#### Accuracy Assessment

The accuracy of VI outputs were then assessed using confusion matrix. Confusion matrix was used

to assess the accuracy of the classification images obtained from the VI processing. The confusion matrix compares the producers and users outputs of image classification and provides the percentage of similarity of the two classification outputs in terms of overall accuracy in percentage. Producer's accuracy is the accuracy of outputs produced by classifier algorithm in the ENVI 4.8 software, meanwhile the user accuracy refers to the ground truth information confirmed by user via ground visual inspection. The overall accuracy is calculated by summing the number of pixels classified correctly based on ground truth and divide by the total number of pixels (Kohavi and Provost, 1998).

The assessment of the classification accuracy is also calculated using the Kappa coefficient by multiplying the total number of pixels in the ground truth classes by the sum of the confusion matrix diagonals; and subtracting the sum of the ground truth pixels in a class times the sum of the classified pixels in that class summed over all classes and dividing by the total number of pixels squared minus the sum of the ground truth pixels in that class times the sum of the classified pixels in that class summed over all classes (Viera and Garrett, 2005). This can assist users to determine the class of classification

**TABLE 5. INTERPRETATION OF KAPPA VALUES WITH RESPECT TO CLASSIFICATION ACCURACY CLASSES**

Kappa value	Classification accuracy class
<0	Poor
0.01-0.20	Slight
0.21-0.40	Fair
0.41-0.60	Moderate
0.61-0.80	Substantial
0.81-0.99	Good

accuracy achieved in this study. The interpretation of Kappa values for classification accuracy classes is shown in *Table 5* (Viera and Garrett, 2005).

The outputs from REP and CR were assessed using t-test. The t-test is a parametric comparative statistical technique that is used to identify whether there is a statistically significant difference between two set of data (Lee Abbott and McKinney, 2013). In this study, the REP and CR from dataset of T1, T2 and T3 were pairwise into three pairs which are T1 vs. T2, T2 vs. T3 and T1 vs. T3 for accuracy assessment. The *p*-value for existence of statistically significant difference between pairwise comparisons was set to 0.05 with 95% confidence level. The t-test was conducted using Sigmapstat 3.5 software (SYSTAT, 2017).

## RESULTS AND DISCUSSION

### Vegetation Indices

The hyperspectral image was analysed using NDVI, SRI, EVI, VREI 1 and CRI 1. The outputs of VI were classified into T1, T2 and T3 using density slicing technique. The classification outputs were assessed for their accuracy via confusion matrix. *Table 6* shows the outputs of five selected VI with their overall accuracy calculated using confusion matrix. The outputs of the VI are in pseudocolour images consisted of T1 (green), T2 (yellow), T3 (red) and non-vegetated (dark). The results showed that SRI has the highest overall accuracy (44.4%) followed by EVI with 40.7% and VOG1 and CRI2 show the same overall accuracy (37%).

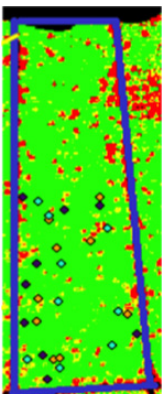
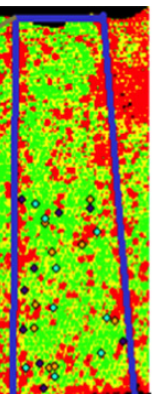
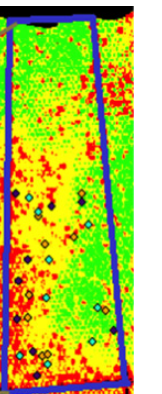
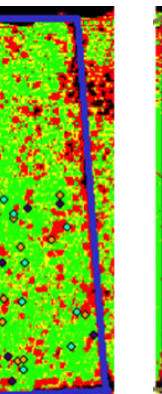
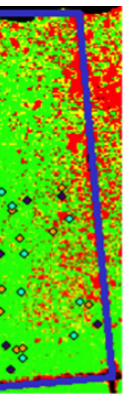
NDVI shows the lowest overall accuracy with the percentage of 33.3%.

From *Table 6*, it can be concluded that the SRI is the best followed by EVI, VOG1, CRI2 and NDVI. But the results also showed that common VI that is usually used for vegetation assessment does not do well for the detection of *Ganoderma* disease in oil palm. This may be due to absence of significant spectral wavelengths that correlate well with *Ganoderma* disease in oil palm as mentioned by Izzuddin (2010), Shafri *et al.* (2011a, b) and Nisfariza (2012).

Further studies should consider the implementation of specific spectral indices suggested by Izzuddin (2010) for detection of *Ganoderma* disease in oil palm seedlings. There are also other works such as from De Castro *et al.* (2015) and Ashourloo *et al.* (2014) that used specific wavelengths and indices for disease detection in crops. De Castro *et al.* (2015) had suggested several wavelength ranges and indices for detection of laurel wilt disease in avocado. Their findings are different from the wavelengths and indices used in this study. These suggested that different diseases require different wavelengths and indices. Leckie *et al.* (2005) suggested that NIR, red and blue bands were most useful. Ratios of bands were notably better than the single bands, with the NDVI or red/near-infrared ratio being the best.

Lelong *et al.* (2010) had conducted hyperspectral data analysis for *Ganoderma* disease detection. They suggested several significant wavelength ranges which are 490 nm - 520 nm, 670 nm - 715 nm, 730 nm - 770 nm and 920 nm - 970 nm which concurred with our findings on the location of significant

TABLE 6. RESULTS OF VEGETATION INDICES CLASSIFICATION

Vegetation index (VI)	NDVI	SRI	EVI	VREI 1	CRI 1
Legend					
T1					
Overall accuracy (%)	33.3	44.4	40.7	37.0	37.0
Kappa	0.000	0.43	0.41	0.056	0.056

Note: T1 - healthy.  
T2 - mild infection.  
T3 - severe infection.

NDVI - Normalised Difference Vegetation Index.  
SRI - Simple Ratio Index.  
EVI - Enhanced Vegetation Index.  
VOG1 - Vogelmann Red Edge Index 1.  
CRI1 - Carotenoid Reflectance Index 1.

wavelengths for the spectral indices development (Izzuddin *et al.*, 2017). Yang *et al.* (2010) suggested the first three principal components from 128 bands (457.2 nm to 921.7 nm) of hyperspectral airborne images for detection of cotton root rot disease in the field. This study showed that the wavelengths used in detection of *Ganoderma* disease are valid to detect infection from root.

### Red Edge Position

The results of hyperspectral image analysis using the REP are shown in *Table 7*. The REP obtained from all four REP techniques are 719.099 nm - 721.397 nm for T1, 718.806 nm - 720.529 nm for T2 and 717.072- 720.771 nm for T3. The REP values of each disease category were arranged for pairwise comparison using t-test. Three pairwise comparison sets were generated for the t-test analysis of REP which were T1 vs. T2, T2 vs. T3 and T1 vs. T3.

*Table 7* shows the descriptive statistics of REP values obtained in this study. The values of the REP for all the three classes in both datasets are similar in mean and statistical analysis failed to detect significant differences between disease categories. These results are contrary with findings by Jiang *et al.* (2010) which suggested that REP went to shorter wavelengths and had significant differences between disease indexes of wheat yellow rust disease. This contradiction may be due to different crop type where oil palm is a perennial crop while wheat is an annual crop with very different physiology. But it can be compared due to changes in foliar properties that also happened when oil palm is infected with *Ganoderma*. The REP technique had also been studied by Shafri and Hamdan (2009) for oil palm and showed good discrimination between healthy and *Ganoderma*-infected oil palm but not in early stage of infection where foliar symptoms is not clearly visible. The REP is not an appropriate indicator because the broader bandwidth of AISA airborne imager hyperspectral image as compared to the handheld sensor of field spectroscopy which has higher spectral resolution.

### Continuum Removal

CR analysis gave different results compared to VI and REP. Two continuum regions were selected

which were located between blue region (400 nm - 550 nm) referred to as 500 nm absorption features and red region (550 nm - 750 nm) termed as 700 nm absorption features. Four CR were tested and the results are shown in *Table 8*. The analyses for image spectra were evaluated based on the visual plots and t-test. The CR values were firstly arranged in three disease categories (T1, T2 and T3) and then were pairwise into three possible pairs (T1 vs. T2, T2 vs. T3 and T1 vs. T3) for t-test assessment.

*Table 8* shows the visual plot and t-test results of the four CR in 500 nm and 700 nm absorption features. The analysis of CR on the 500 nm and 700 nm absorption regions showed that none of CR techniques were capable to completely differentiate T1, T2 and T3 statistically. But the results showed that each of CR technique had their own capability to differentiate some of disease category pairs.

*Table 8* shows that BDNA techniques exhibit a significance difference between both T1 vs. T2 and T1 vs. T3 in the 500-nm absorption region but only can differentiate T1 vs. T3 in the 700 nm absorption region. Meanwhile, in 700 nm absorption regions, there are significant differences for T1 vs. T3 and T2 vs. T3 that accumulate from 643 nm to 714 nm absorption region for all CR, but they cannot distinguish between T1 vs. T2.

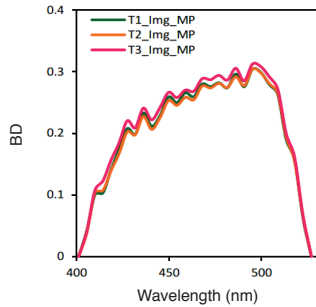
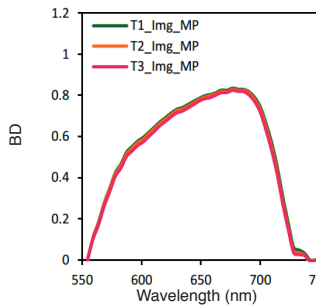
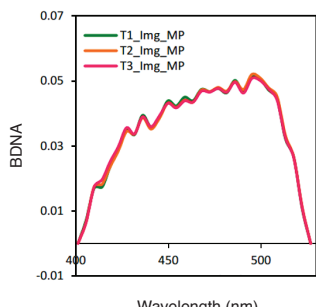
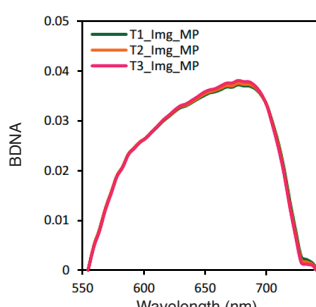
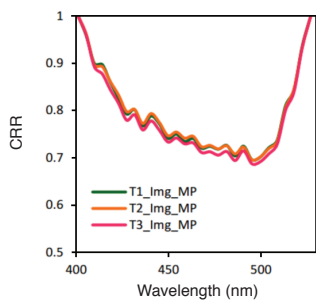
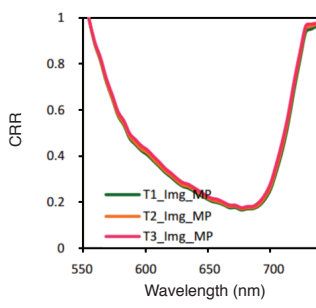
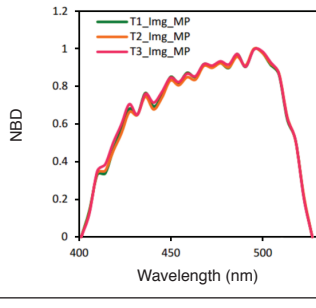
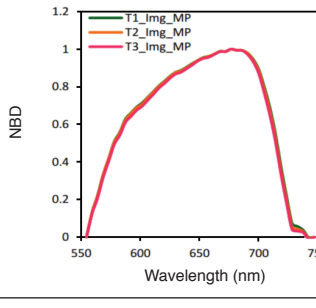
The results from CR analysis showed promising results in detection of early infection of *Ganoderma* disease in oil palm. But it is noted that BDNA in the 500 nm absorption region does not seem capable to differentiate between T2 vs. T3 due to unknown causes. Theoretically, the results may be due to the technique which was not sensitive to detect reduction of stomatal conductance caused by root infection of *Ganoderma* pathogen in the field (Haniff *et al.*, 2005). Other than that, bi-directional reflectance distribution also may cause problem to detect subtle changes of spectral properties between healthy and early infection of *Ganoderma* disease in oil palm. This is due to BRDF effects which are often considered as noise due to the variation in reflectance across an image (*i.e.*, cross-track brightness gradients), even if the cover type is constant. This is a particularly important issue with airborne data when multiple flight lines are mosaicked into a single scene, which is often necessary for mapping at larger spatial scales (Colgan *et al.*, 2012).

TABLE 7. THE DESCRIPTIVE STATISTICS OF THE RED EDGE POSITION (REP)

Ganoderma disease severity index	Minimum	Maximum	Range	Mean	Standard deviation	Variance
T1	719.099	721.397	2.298	720.023	0.695	0.484
T2	718.806	720.529	1.723	719.587	0.570	0.325
T3	717.072	720.771	3.698	719.097	1.035	1.072

Note: T1 – healthy. T2 – mild infection. T3 – severe infection.

TABLE 8. RESULTS OF CONTINUUM REMOVAL ANALYSIS

Continuum removal (CR)	500 nm absorption			700 nm absorption		
Band Depth (BD)						
t-test	A X	B X	C X	A X	B X	C O
Band Depth Normalised to Area (BDNA)						
t-test	A O	B X	C O	A X	B X	C O
Continuum Removed Reflectance (CRR)						
t-test	A X	B X	C X	A X	B X	C O
Normalised Band Depth (NBD)						
t-test	A X	B X	C X	A X	B O	C O

Note: Results for t-test - O (significant difference); and X (no significant difference).

p-value - 0.05 with 95% confidence level.

T1 - healthy, T2 - mild infection, T3 - severe infection.

A - T1 vs. T2, B - T2 vs. T3, C - T1 vs. T3.

Analysis on CR of 700 nm absorption showed that all CR can distinguish between T1 vs. T3 significantly. But more experiments must be conducted to solve the question on why there are lacks of significant differences between T2 vs. T3 in CR analysis. Perhaps BRDF effect really needs to be conducted in future works to reduce the spectral fluctuations and overlap. Finally, the results suggested that there is opportunity in terms of detection of early infection of *Ganoderma* disease in mature oil palm but requires further extensive validation with emphasis on BRDF effects during the airborne hyperspectral image acquisition.

### CONCLUSION AND RECOMMENDATION

The AISA Dual airborne hyperspectral image had been analysed using three spectral analysis methods *i.e.* VI, REP ad CR. The methods were used to classify oil palm into three *Ganoderma* DSi namely T1, T2 and T3. Category T2 is considered as early symptom (mild infection) of *Ganoderma* disease in oil palm. The results showed difference performance of each methods in classification of the disease severity categories. The VI showed low to moderate (30%-40%) percentage of accuracy for classification of the *Ganoderma* DSi. The REP also showed unsuccessful discrimination between the three *Ganoderma* DSi. Nevertheless, CR had shown promising results when t-test analysis showed significant difference between pairwise comparison of T1 vs. T2 and T1 vs. T3. But in-depth analysis such as image transformation using wavelet analysis and classification of indices output using advance classification techniques such as Support Vector Machine and Neural Networks should be conducted for future works to identify the causes for the inability to differentiate T2 vs. T3 using the CR analysis. Hypothetically, the reason is that the BRDF effect during the image acquisition is not included in the analysis of the airborne hyperspectral image. For future works, extensive experiment of collecting BRDF data using goniometer during airborne hyperspectral image acquisition is needed to acquire better understanding of spectral signatures between healthy and *Ganoderma* infected oil palm.

### ACKNOWLEDGEMENT

We would like to thank the Director-General of MPOB for permission to publish this article and the staff of GanoDROP Unit, MPOB for their support and commitment on this study. This project was conducted with support from the Universiti Malaya Research Grant (UMRG) - Innovative Technology Research Cluster (ITRC): RP023-2012E.

### REFERENCES

- ASHOURLOO, D; MOBASHERI, M and HUETE, A (2014). Evaluating the effect of different wheat rust disease symptoms on vegetation indices using hyperspectral measurements. *Remote Sensing*, 6: 5107-5123.
- BONHAM-CARTER, G F (1988). Numerical procedures and computer program for fitting an inverted Gaussian model to vegetation reflectance data. *Computers and Geosciences*, 14: 339-356.
- CALDERON, R; NAVAS-CORTES, J A; LUCENA, C and ZARCO-TEJADA, P J (2013). High-resolution airborne hyperspectral and thermal imagery for early detection of Verticillium wilt of olive using fluorescence, temperature and narrow-band spectral indices. *Remote Sensing Environment*, 139: 231-245.
- CARTER, G A and KNAPP, A K (2001). Leaf optical properties in higher plants: Linking spectral characteristics to stress and chlorophyll concentration. *American J. Botany*, 88: 677-684.
- CHO, M A and SKIDMORE, A K (2006). A new technique for extracting the red edge position from hyperspectral data: The linear extrapolation method. *Remote Sensing of Environment*, 101: 181-193.
- CLARK, R N (2003). Imaging spectroscopy: Earth and planetary remote sensing with the USGS Tetracorder and expert systems. *J. Geophysical Research*, 108: 1-2.
- CLARK, R N and ROUSH, T L (1984). Reflectance spectroscopy: Quantitative analysis techniques for remote sensing applications. *J. Geophysical Research: Solid Earth*, 89: 6329-6340.
- CLEVERS, J G P W (1994). Imaging spectrometry in agriculture – Plant vitality and yield indicators. *Imaging Spectrometry - A Tool for Environmental Observations* (Hill, J and Mégier, J eds.). Dordrecht: Springer, Netherlands. p. 193-219.
- CLEVERS, J G P W and GITELSON, A A (2013). Remote estimation of crop and grass chlorophyll and nitrogen content using red-edge bands on Sentinel-2 and -3. *Int. J. App. Earth Obs. and Geoinfo.* 23: 344-351.
- COLGAN, M S; BALDECK, C A; FERRET, J and ASNER, G P (2012). Mapping savanna tree species at ecosystem scales using support vector machines classification and BRDF correction on airborne

- hyperspectral and LiDAR data. *Remote Sensing*, 4: 3462-3480.
- DAUGHTRY, C S T; WALTHALL, C L; KIM, M S; BROWN DE COULSTOUN and McMURTRY III, J E (2000). Estimating corn leaf chlorophyll concentration from leaf and canopy reflectance. *Remote Sensing of Environment*, 74: 229-239.
- DAWSON, T P and CURRAN, P (1998). A new technique for interpolating the reflectance red edge position. *International J. Remote Sensing*, 19: 2133-2139.
- DE CASTRO, A I; EHSANI, R; PLOETZ, R C; CRANE, J H and BUCHANON, S (2015). Detection of laurel wilt disease in avocado using low altitude aerial imaging. *PLoS ONE*, 10: e0124642. <https://doi.org/10.1371/journal.pone.0124642>
- FILELLA, I and PENUELAS, J (1994). The red edge position and shape as indicator of plant chlorophyll content, biomass and hydric status. *International J. Remote Sensing*, 15: 1459-1470.
- FILIMON, R V; ROTARU, L and FILIMON, R M (2016). Quantitative investigation of leaf photosynthetic pigments during annual biological cycle of *Vitis vinifera* L. Table grape cultivars. *South African J. Enology and Viticulture*, 37: 1-14.
- FRANKE, J; MENZ, G; OERKE, E C and RASCHER, U (2005). Comparison of multi- and hyperspectral imaging data of leaf rust infected wheat plants. *Proc. of the SPIE 5976, Remote Sensing for Agriculture, Ecosystems, and Hydrology VII* (Owe, M and D'Urso, G B eds.). SPIE, Belgium. 11 pp.
- GITELSON, A A; ZUR, Y; CHIVKUNOVA, O B and MERZLYAK, M N (2002). Assessing carotenoid content in plant leaves with reflectance spectroscopy. *Photochemistry and Photobiology*, 75: 272-281.
- GITELSON, A A; VIÑA, A; CIGANDA, V; RUNDQUIST, D C and ARKEBAUER, T J (2005). Remote estimation of canopy chlorophyll content in crops. *Geophysical Research Letters*, 32: DOI:10.1029/2005GL022688.
- GUPTA, R S (2010). Molecular signatures for the main phyla of photosynthetic bacteria and their subgroups. *Photosynthesis Research*, 104: 357-372.
- GUYOT, G; BARET, F and JACQUEMOND, S (1992). Imaging spectroscopy for vegetation studies. *Imaging Spectroscopy: Fundamentals and Prospective Applications* (Toselli, F and Bodechtel, J eds.). Brussels and Luxembourg: Springer Netherlands. p. 145-165.
- HABOUDANE, D; MILLER, J R; TREMBLAY, N; ZARCO-TEJADA, P J and DEXTRAZE, L (2002). Integrated narrow-band vegetation indices for prediction of crop chlorophyll content for application to precision agriculture. *Remote Sensing of Environment*, 81: 416-426.
- HANIFF, M H; ISMAIL, S and IDRIS, A S (2005). Gas exchange responses of oil palm to *Ganoderma boninense* infection. *Asian J. Plant Sciences*, 4: 438-444.
- IDRIS, A S; NUR RASHYEDA, R; MOHD HEFNI, R; SHAMALA, S and NORMAN, K (2016). *Standard Operating Procedures (SOP) Guidelines for Managing Ganoderma Disease in Oil Palm*. MPOB, Bangi, Malaysia. 41 pp.
- IZZUDDIN, M A (2010). *Early Detection of Ganoderma Disease in Oil Palm (Elaeis guineensis Jacq) Using Field Spectroscopy*. M.Sc thesis, Universiti Putra Malaysia, Selangor, Malaysia.
- IZZUDDIN, M A; IDRIS, A S; NISFARIZA, M N; NORDIANA A A; SHAFRI, H Z M and EZZATI, B (2017). The development of spectral indices for early detection of *Ganoderma* disease in oil palm seedlings. *International J. Remote Sensing*, 38: 6505-6527.
- JIANG, J B; CHEN, Y H and HUANG, W J (2010). Using the distance between hyperspectral red edge position and yellow edge position to identify wheat yellow rust disease. *Spectroscopy and Spectral Analysis*, 30: 1614-1618.
- JORDAN, C F (1969). Derivation of leaf-area index from quality of light on the forest floor. *Ecology*, 50: 663-666.
- KOHAVI, R and PROVOST, F (1998). On applied research in machine learning. *Machine Learning*, 10: 1-6.
- KOKALY, R F and CLARK, R N (1999). Spectroscopic determination of leaf biochemistry using band-depth analysis of absorption features and stepwise multiple linear regression. *Remote Sensing of Environment*, 67: 267-287.
- KREZHOVA, D; DIKOVA, B and MANEVA, S (2014). Ground based hyperspectral remote sensing for disease detection of tobacco plants. *Bulgarian J. Agricultural Science*, 20: 1142-1150.
- LECKIE, D G; CLONEY, D and JOYCE, S P (2005). Automated detection and mapping of crown discolouration caused by Jack Pine budworm with 2.5 m resolution multispectral imagery. *International J. Applied Earth Observation and Geoinformation*, 5: 61-77.

- LEE ABBOTT, M and MCKINNEY, J (2013). Statistical methods of difference: T test. *Understanding and Applying Research Design*. New Jersey: John Wiley and Sons.
- LELONG, C C D; ROGER, J M; BREGAND, S; DUBERTRET, F; LANORE, M; SITORUS, N A; RAHARJO, D A and CALIMAN, J P (2010). Evaluation of oil-palm fungal disease infestation with canopy hyperspectral reflectance data. *Sensors*, 10: 734-747.
- LIU, H Q and HUETE, A (1995). A feedback based modification of the NDVI to minimize canopy background and atmospheric noise. *IEEE Transactions on Geoscience and Remote Sensing*, 33: 457-465.
- MADIHAH, A Z; IDRIS, A S and RAFIDAH, A R (2014). Polyclonal antibodies of *Ganoderma boninense* isolated from Malaysia oil palm for detection of basal stem rot disease. *African J. Agricultural Research*, 13: 3455-3463.
- MAHLEIN, A K; STEINER, U; DEHNE, H W and OERKE, E C (2010). Spectral signatures of sugar beet leaves for the detection and differentiation of diseases. *Precision Agriculture*, 11: 413-431.
- MILLER, J R; HARE, E W and WU, J (1990). Quantitative characterization of the vegetation red edge reflectance 1. An inverted-Gaussian reflectance model. *International J. Remote Sensing*, 11: 1755-1773.
- MUTANGA, O and SKIDMORE, A K (2003). Continuum-removed absorption features estimate tropical savanna grass quality *in situ*. *3<sup>rd</sup> EARSEL Workshop on Imaging Spectroscopy*. May 2003, Herrsching, Germany: DLR. p. 13-16.
- NISFARIZA, M N (2012). *Early Detection of Ganoderma Basal Stem Rot Disease of Oil Palm by HYPERSPECTRAL REMOTE Sensing*. Ph.D thesis, University of Nottingham, United Kingdom.
- NURANIS, I; KAMARUZAMAN, S; KHAIRULMAZMI, A; MOHD SHUKRI, I; ZULKIFLI, H and IDRIS, A S (2016). Leaf nutrient status in relation to severity of *Ganoderma* infection in oil palm seedlings artificially infected with *Ganoderma boninense* using root inoculation technique. *Oil Palm Bulletin No.* 72: 25-31.
- PHADIKAR, S and GOSWAMI, J (2016). Vegetation indices based segmentation for automatic classification of brown spot and blast diseases of rice. *Recent Advances in Information Technology (RAIT), 2016 3<sup>rd</sup> International Conference*. 3-5 March 2016, Dhanbad, India. DOI: 10.1109/RAIT.2016.7507917.
- REES, W G (2013). *Physical Principles of Remote Sensing*. 3<sup>rd</sup> ed. Cambridge University Press.
- ROGGE, D M; RIVARD, B; ZHANG, J; SANCHEZ, A; HARRIS, J and FENG, J (2007). Integration of spatial-spectral information for the improved extraction of endmembers. *Remote Sensing of Environment*, 110: 287-303.
- ROSLAN, A and IDRIS, A S (2012). Economic impact of *Ganoderma* incidence on Malaysian oil palm plantation - A case study in Johor. *Oil Palm Industry Economic J. Vol.* 12: 24-30.
- ROUSE, J W; HAAS, R H; SCHELL, J A and DEERING, D W (1973). Monitoring vegetation systems in the Great Okains with ERTS. *3<sup>rd</sup> Earth Resources Technology Satellite-1 Symposium*. December 1973. Washington D.C., USA: p. 325-333.
- SANKARAN, S and EHSANI, R (2011). Visible-near infrared spectroscopy based citrus greening detection: Evaluation of spectral feature extraction techniques. *Crop Protection*, 30: 1508-1513.
- SHAFRI, H Z M; IZZUDDIN, M A and SARIPAN, M I (2009). Modified vegetation indices for *Ganoderma* disease detection in oil palm from field spectroradiometer data. *J. Applied Remote Sensing*, 3: 23.
- SHAFRI, H Z M and HAMDAN, N (2009). Hyperspectral imagery for mapping disease infection in oil palm plantation using vegetation indices and red edge techniques. *American J. Applied Sciences*, 6: 1031-1035.
- SHAFRI, H Z M; IZZUDDIN, M A; IDRIS A S and NISFARIZA, M N (2011a). Spectral discrimination of healthy and *Ganoderma*-infected oil palms from hyperspectral data. *International J. Remote Sensing*, 32: 7111-7129.
- SHAFRI, H Z M; HAMDAN, N and SARIPAN, M I (2011b). Semi-automatic detection and counting of oil palm trees from high spatial resolution airborne imagery. *International J. Remote Sensing*, 32: 2095-2115.
- SYSTAT (2017). Sigmastat. from: <https://systatsoftware.com/products/sigmastat/>, accessed on 29 January 2017.
- VIERA, AJ and GARRETT, JM (2005). Understanding interobserver agreement: The Kappa statistic. *Family Medicine*, 37: 360-363.

VINCINI, M and FRAZZI, E (2011). Comparing narrow and broad-band vegetation indices to estimate leaf chlorophyll content in planophile crop canopies. *Precision Agriculture*, 12: 334-344.

VOGELMANN, J E; ROCK, B N and MOSS, D M (1993). Red edge spectral measurements from sugar maple leaves. *International J. Remote Sensing*, 14: 1563-1575.

WU, C; NIU, Z; TANG, Q; HUANG, W; RIVARD, B and FENG, J (2009). Remote estimation of gross primary production in wheat using chlorophyll-related vegetation indices. *Agricultural and Forest Meteorology*, 149: 1015-1021.

YANG, C; EVERITT, J H and FERNANDEZ, C J (2010). Comparison of airborne multispectral and hyperspectral imagery for mapping cotton root rot. *Biosystems Engineering*, 107: 131-139.

XING, J; BRAVO, C; JANCSÓK, P T; RAMON, H and DE BAERDEMAEKER, J (2005). Detecting bruises on 'Golden Delicious' apples using hyperspectral imaging with multiple wavebands. *Biosystems Engineering*, 90: 27-36.

ZHAO, Y-R; LI, X; YU, K-Q; CHENG, F and HE, Y (2016). Hyperspectral imaging for determining pigment contents in cucumber leaves in response to angular leaf spot disease. *Scientific Reports*, 6: 27790. DOI:10.1038/srep27790.